IEEE Access
Multidisciplinary : Rapid Review : Open Access Journal

Received May 29, 2020, accepted June 20, 2020, date of publication June 29, 2020, date of current version July 7, 2020.

Digital Object Identifier 10.1109/ACCESS.2020.3005628

Three Phase Four-Wire Inverter for Grid-Disconnected Operation

VIRGILIO VÁSQUEZ[1], RUBÉN ORTEGA[2,3], LUIS MAURO ORTEGA[1], VÍCTOR HUGO GARCÍA[2], AND OSCAR CARRANZA[2,3], (Member, IEEE)

[1] Instituto Tecnológico de Estudios Superiores de Monterrey, Tecnológico de Monterrey, Atizapán 52926, Mexico
[2]Escuela Superior de Cómputo, Instituto Politécnico Nacional, Ciudad de Mexico 07838, Mexico
[3]Escuela Superior de Ingeniería Mecánica y Eléctrica, Instituto Politécnico Nacional, Ciudad de Mexico 07738, Mexico

Corresponding author: Rubén Ortega (rortegag@ipn.mx)

This work was supported by the Comisión de Operación y Fomento de Actividades Académicas del Instituto Politécnico Nacional.

ABSTRACT In this work, the modeling of a three-phase four wires inverter and the design of two control schemes for its grid-disconnected operation are presented. The advantages of the four-wire topology are that by means of a coordinate transformation (Park transformation) it is possible to obtain a decoupled linear model, as well as feeding single-phase and three-phase loads in this operating mode. In the model, two control loops are taken into account: a current loop (controller slave) and a voltage loop (controller master) with the aim that this inverter can regulate its output voltage and when it is supplied to a local load.. The contributions of this work is present in the inverter modeling, the method for obtaining the transfer functions and in the controllers design obtained by this method. The inverter model allows to easily obtain the transfer functions of both loops; this is very important for the control area, considering that using classical control techniques and the methodology proposed in this work, the gains can be obtained directly and not adjusted to trial and error. The main advantage of this proposal is that when the kp and ki gains are obtained through the Bode diagrams, we can obtain generalized integrators; applying the coordinate transformation method to the integral gain that was obtained by the design of the PI controller in direct current (dc); This method is described in detail in the presented work and allows obtaining a new controller called proportional controller plus generalized integrator (P+GI). This controller presents a good performance, since it can follow sinusoidal references, in addition to presenting a better disturbances rejection due to the high gains it presents at the grid frequency and harmonic frequencies of the load.

INDEX TERMS Inverter, grid-disconnected mode, microgrid, park transformation, PI controller, generalized integrator.

I. INTRODUCTION

Technological development has led to a gradual change in the way that modern societies have developed, causing a significant increase in energy demand per inhabitant per year. In this context, until a few years ago, conventional forms of power generation associated with fossil fuel consumption proved to be a solution to this change. Although this increase and this strategy of energy generation have improved the welfare of the different consumer societies, it is convenient to take into account all the possible elements when evaluating their impact on our quality of life. An example of this is the environmental impact of the processes used to generate the demanded energy and the scarcity of the available resources.

Today, it is observed that oil production reached its peak while gas production will reach it around the year 2030. In this context, a strong increase in energy prices is expected, according to studies published by the Global Wind Energy Council (GWEC) and Renewable Energy Systems Limited (RESL) [1]. That is why several solutions are brought into play in the debate that aims to modify the energy production scenario in the future. Within this framework, the so-called renewable energies are currently present as a possible, ecological and profitable option capable of satisfying the energy needs of different societies in different parts of the world.

The renewable concept is related to the regeneration capacity of energy sources, so that those sources whose

The associate editor coordinating the review of this manuscript and approving it for publication was Qi Zhou.

This work is licensed under a Creative Commons Attribution 4.0 License. For more information, see https://creativecommons.org/licenses/by/4.0/

regeneration rate is much higher than the utilization rate can be considered as such. Within this group are solar, wind, hydraulic, geothermal or biomass energy, to name the most important. Like fossil fuels, renewable energy sources are not distributed evenly throughout the planet, so that each country can find in its environment the most appropriate renewable resource for the generation of electricity. This alternative will reduce the dependence on the generation of energy with conventional sources. A characteristic that places them in an advantageous position in the future environment of the generation and distribution of energy. Because many of the conversion systems used in renewable energies are modular, it is easy to integrate them into the microgrids that make up the generation systems [2], [3]. This guarantees a higher quality and reliability in the energy consumed [4]–[8].

Taking into account that solar energy systems have proliferated significantly in recent years, as shown by the data from the IEA Photovoltaic Energy Systems Program [9], in this research work, solar energy is the source of renewable energy. So, the existence of a photovoltaic generation installation (IGF) is considered. The authors in [9] show that solar energy has had an exponential evolution in installed power throughout the world, so the scientific community is studying the improvement of these systems, necessary to maintain this growth trend.

An element that plays a very important role is the inverter, which act as a means of interconnection between the renewable source, the load and/or the grid, its objective is to generate a sinusoidal signal that is delivered to the load and/or inject into the grid. Considering this point, this document proposes the modeling and design of a three-phase four-wire inverter to operate in grid-disconnected mode. In addition, in this application two controllers are proposed. They allow fulfilling the objective of maintaining the amplitude of the waveform and the frequency of the voltage signal that will be delivered to the load.

In the literature there are published works where models of three-phase four wires inverters have been developed using the Park transformation matrix that allows obtaining a decoupled model [10], [11]. These ideas are still used in the present, proof of this are the papers presented in [12] and [13]. In [12] for example, a controller is designed for the voltage loop of a four-wire inverter but the design of a controller for the current loop is not considered. In [13], the results obtained can be compared with those obtained in the present work where it is observed that in the simulation tests for presented linear load, a THD value of 1.2% was reported for the converter output voltage signal. Particularly, in the work that is being presented, the THD for the voltage signal with linear load is 0.9%, that is, lower. In addition, results with non-linear load are presented and the results with the proposed controller (P+3GI) turn out to be very good with a THDv of 2.2%.

In the reviewed works [14]–[16]; where is propose two control schemes: a proportional-integral control scheme (PI) for both loops: current - voltage and a second control scheme based on symmetric components for both loops. The second scheme is designed due to the low performance shown by the classic PI control schemes; however, they do not present the design of these controllers. In [17], the authors propose control schemes PR (Proportional-Resonant) also for both loops. These control schemes PR are proposed due to the difficulties of using proportional-integral control schemes for the tracking of setpoints of alternating current signals [18]. In the control schemes design, the authors present a frequency analysis using the closed loop transfer functions for positive and negative sequences, this is confusing since the gain values of both controllers are not known. In general, open loop calculation is used for the design of these control schemes to obtain the closed loop. In [19], the authors propose three control schemes PI (Proportional-integral), PR (Proportional-Resonant) and DB (Dead-beat). Where they obtain by algebraic means the transfer function that allows to obtain the gains of the PI controller and use them for the PR controller. In the gain calculation of the PR controller design, they use the root locus theory technique to adjust the proportional gain k_p and subsequently, with the obtained k_p gain, they use the Bode diagram with different values of the integral gain k_i to select the best value that provides a high gain to the resonant frequency of the controller. This design methodology is not clear since to apply the root locus theory technique, it is necessary to set one of the two gains k_p and/or k_i. The authors never present the method that allowed them to obtain the value of k_i and k_p. That is, from performing several tests randomly they obtained the best value of k_i. In the design of the DB controller, the authors recommend the following method "increase artificially the gain b of the controller in respect to its initial value calculated". In [20] a novel blended state estimated adaptive controller is designed for voltage and current control of microgrid against unknown noise. An adaptive PID controller is also developed and used in system conjunction with the estimator to regulate its voltage and current against the number of loads. Deviation in load parameters hamper the function of the microgrid system. The performance of the developed controller is also evaluated against number of loads. Results indicate the controller provides a more stable and high-tracking performance with the inclusion of the unscented Kalman filter (UKF) in the system. In [21] is presents the independent control design per phase for PV three-phase four-wire inverters, which are able to inject different active and reactive powers in each phase, in order to reduce the system phase unbalance is considered

The contributions of this work is present in the inverter modeling, the method for obtaining the transfer functions and in the controllers design obtained by this method. In particular, a current loop and a voltage loop are considered in the inverter model; which allows to clearly obtain the transfer functions of both loops. For the controllers design of both loops, the coordinate transformation method is used, which allows controllers designing in ac from the controllers design in dc. It is highlighted that when taking into account the two inverter control loops, it can work both in grid-connected and

grid-disconnected from it. However, in this work its design is given for grid-disconnected operation.

Another important aspect in this work, it is the controller design called proportional controller add generalized integrator (P+GI) [22]–[24].

Particularly, the control configuration used in this application is obtained initially from the PI control design [25] in direct current (*dc*) and through a process of coordinate transformation that is applied to the integral action. The main advantage provided by this controller is the disturbances rejection and to have a better setpoint tracking, that may occur when the inverter is in grid-disconnected mode. A generalized integrator can provide high gains to the frequency of the grid and the harmonics frequency derived from different types of loads, so it turns out to be a suitable solution for the disturbances rejection (Total Harmonic Distortion THDv) characteristic of the grid and of different types of loads [26].

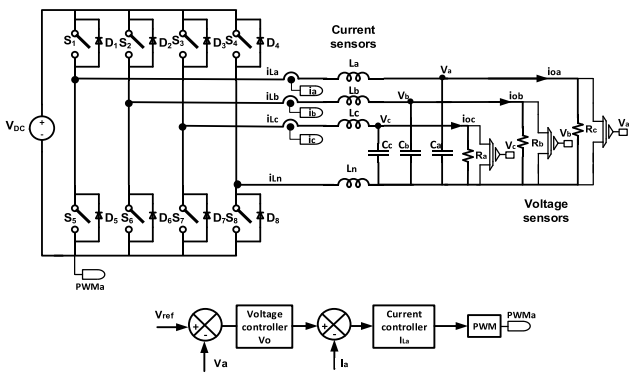

FIGURE 1. Three phase four-wire inverter.

Fig. 1 shows the structure of the four-wire inverter. In applications in grid-disconnected operation, the inverter has an LC low pass filter at its output. The filter has the purpose of attenuating the high voltage switching frequencies and the current undulations. The fourth wire representing the neutral wire is connected at the point where the three phases *a, b* and *c* are interconnected. The neutral wire inductor L_n allows reducing the ripple of the switching current and limit the fault current in short-circuit conditions [27], [28]. Therefore, it is highly recommended to use the inductor filter of the fourth leg.

The four-wire inverter requires two additional power switches, as well as gate control circuits, so the modulation and control technique used is can be more complex [26]–[29].

As mentioned above, control techniques that achieve high performance of the four-legged inverter under different conditions linear/non-linear load and balanced/unbalanced are required. Several models and methods of scheme controllers of the four-legged inverter are reported in the literature [30]–[36].

A four-wire inverter has the following advantages: it allows feeding three-phase and single-phase loads in addition to supporting load imbalance; since in neutral thread the currents derived from the imbalance can circulate maintaining a good performance, as it is observed in the tests obtained by means of simulations.

It is worth mentioning that any source of direct current (*dc*) energy such as renewable energies, storage devices or *ac/dc* converters can be connected to the inverter input, all of them represented by direct current sources (V_{DC}), as shown in Fig. 1. In this figure, it is also presented the sensing of the current and voltage signals as well as the control structure used.

This work is organized as follows: the second section presents the model in state variables, development and description. In section three is presented the master-slave control schemes design. In section four, the results obtained from the inverter performance are presented, through simulations. In section five, the results discussion obtained through simulations are presented and finally in section six the work conclusions are presented.

In the following section, the four-wire inverter model is developed and described in state variables. This work highlights the inclusion of the inductor in the fourth wire or neutral wire, which is considered for the regulators design of the current and voltage loops current and voltage loops that integrate the inverter

II. MODEL IN STATE VARIABLES, DEVELOPMENT AND DESCRIPTION

To obtain the inverter model, it is considering a phase by shown in Fig. 2.

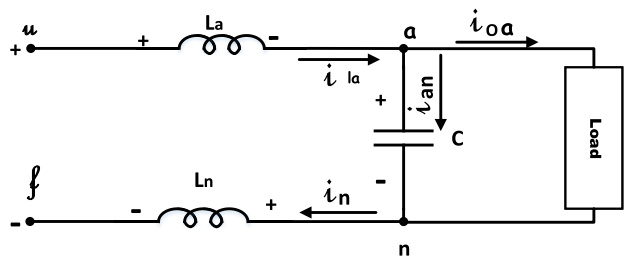

FIGURE 2. Representation of a phase of the inverter circuit.

Applying Kirchhoff's voltage law to the electrical circuit shown in Fig 2, the expression (1) is obtained by.

$$-V_{uf} + V_{La} + V_{an} + V_{Ln} = 0 \tag{1}$$

The expressions show the inductors voltages:

$$V_{La} = L_a \frac{di_{La}(t)}{dt} \text{ and } V_{Ln} = L_n \frac{di_n(t)}{dt}$$

It is possible rewrite the equation (1) as follows:

$$L_a \frac{di_{La}(t)}{dt} + L_n \frac{di_n(t)}{dt} = V_{uf} - V_{an}$$

Following this procedure for the phases *uf* and *wf* the differential equations that describe the inverter input circuit

are obtained by.

$$\begin{bmatrix} L & 0 & 0 \\ 0 & L & 0 \\ 0 & 0 & L \end{bmatrix} \frac{d}{dt} \begin{bmatrix} i_{La} \\ i_{Lb} \\ i_{Lc} \end{bmatrix} + L_n \frac{d}{dt} \begin{bmatrix} i_n \\ i_n \\ i_n \end{bmatrix} = \begin{bmatrix} V_{uf} \\ V_{vf} \\ V_{wf} \end{bmatrix} - \begin{bmatrix} V_{an} \\ V_{bn} \\ V_{cn} \end{bmatrix} \tag{2}$$

where $L_a = L_b = L_c = L$ is considered.

Applying the Kirchhoff currents law to the inverter output node, in particular to node a in the Fig. 2, it is obtained by.

$$i_{La} = i_{an} + i_{oa}$$

where i_{an} is the current flowing through the capacitor and i_{oa} is the current flowing through the load. In particular, the current i_{an} is expressed by.

$$i_{an} = C\frac{dV_{an}}{dt}$$

The above expression is written by:

$$i_{La} - i_{oa} = C\frac{dV_{an}}{dt}$$

Applying the same procedure for phases vf and wf it is possible to obtain the inverter phase output circuit model.

$$\begin{bmatrix} C & 0 & 0 \\ 0 & C & 0 \\ 0 & 0 & C \end{bmatrix} \frac{d}{dt} \begin{bmatrix} V_{an} \\ V_{bn} \\ V_{cn} \end{bmatrix} = \begin{bmatrix} i_{La} \\ i_{Lb} \\ i_{Lc} \end{bmatrix} - \begin{bmatrix} i_{oa} \\ i_{ob} \\ i_{oc} \end{bmatrix} \tag{3}$$

Consider now the three phases diagram in the inverter output shown in Fig. 3.

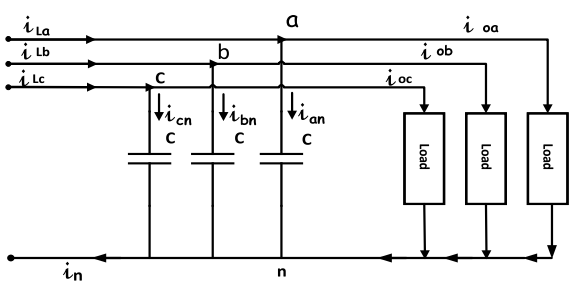

FIGURE 3. Inverter output circuit.

Applying the Kirchhoff currents law in the nodes a, b, c.

$$i_{oc} = i_{Lc} - i_{cn}, \quad i_{ob} = i_{Lb} - i_{bn}, \; i_{oa} = i_{La} - i_{an}$$

where i_{an}, i_{bn} e i_{cn} are the currents that circulate for each capacitor of each inverter phase, i_{oa}, i_{ob} e i_{oc} are the currents that circulate through the loads. The sum of currents in node n is given by.

$$i_{oc} + i_{ob} + i_{oa} + i_{cn} + i_{bn} + i_{an} = i_n$$

Substituting the relations of the currents flowing through the loads of each inverter phase i_{oa}, i_{ob} and i_{oc}, the relation of the currents at output node is obtained by.

$$i_{Lc} + i_{Lb} + i_{La} = i_n \tag{4}$$

Substituting (4) in (2) and performing the operations for each row of the matrix differential equation (2) for better tracking of expressions, operations are performed for one row.

$$L\frac{di_{La}(t)}{dt} + L_n\frac{di_n(t)}{dt} = V_{uf} - V_{an}$$
$$L\frac{di_{La}(t)}{dt} + L_n\frac{d}{dt}[i_{Lc} + i_{Lb} + i_{La}] = V_{uf} - V_{an}$$
$$(L + L_n)\frac{di_{La}(t)}{dt} + L_n\frac{di_{Lb}}{dt} + L_n\frac{di_{Lc}}{dt} = V_{uf} - V_{an}$$

Following the same procedure for each of the rows in equation (2), the inverter currents model as a function of the supply and inverter output voltages is obtained by.

$$L_{eq}\frac{d}{dt}\begin{bmatrix} i_{La} \\ i_{Lb} \\ i_{Lc} \end{bmatrix} = \begin{bmatrix} V_{uf} - V_{an} \\ V_{vf} - V_{bn} \\ V_{wf} - V_{cn} \end{bmatrix}$$
$$\frac{d}{dt}\begin{bmatrix} i_{La} \\ i_{Lb} \\ i_{Lc} \end{bmatrix} = L_{eq}^{-1}\begin{bmatrix} V_{uf} - V_{an} \\ V_{vf} - V_{bn} \\ V_{wf} - V_{cn} \end{bmatrix} \tag{5}$$

where the matrix L_{eq} and L_{eq}^{-1} are given by.

$$L_{eq} = \begin{bmatrix} L + L_n & L_n & L_n \\ L_n & L + L_n & L_n \\ L_n & L_n & L + L_n \end{bmatrix}$$

$$L_{eq}^{-1} = \frac{1}{L + L_n}\begin{bmatrix} 1 + \frac{2L_n}{L} & -\frac{L_n}{L} & -\frac{L_n}{L} \\ -\frac{L_n}{L} & 1 + \frac{2L_n}{L} & -\frac{L_n}{L} \\ -\frac{L_n}{L} & -\frac{L_n}{L} & 1 + \frac{2L_n}{L} \end{bmatrix}$$

Finally, equations (3) and (5) describe the inverter dynamic behavior.

The following subsection presents the development of the decoupling of equations of state.

A. DECOUPLING OF STATE EQUATIONS

Applying the Park transformation matrix that allows transforming the uvw reference system to a reference system $\alpha\beta\gamma$ given by.

$$\begin{bmatrix} v_{\alpha f} \\ v_{\beta f} \\ v_{\gamma f} \end{bmatrix} = T\begin{bmatrix} V_{uf} \\ V_{vf} \\ V_{wf} \end{bmatrix}; \begin{bmatrix} v_{\alpha n} \\ v_{\beta n} \\ v_{\gamma n} \end{bmatrix} = T\begin{bmatrix} V_{an} \\ V_{bn} \\ V_{cn} \end{bmatrix}$$
$$\begin{bmatrix} i_{L\alpha} \\ i_{L\beta} \\ i_{L\gamma} \end{bmatrix} = T\begin{bmatrix} i_{La} \\ i_{Lb} \\ i_{Lc} \end{bmatrix}; \begin{bmatrix} i_{o\alpha} \\ i_{o\beta} \\ i_{o\gamma} \end{bmatrix} = T\begin{bmatrix} i_{oa} \\ i_{ob} \\ i_{oc} \end{bmatrix} \tag{6}$$

where the transformation matrix T and T^{-1} are given by.

$$T = \frac{2}{3}\begin{bmatrix} 1 & \frac{-1}{2} & \frac{-1}{2} \\ 0 & \frac{\sqrt{3}}{2} & \frac{-\sqrt{3}}{2} \\ \frac{1}{2} & \frac{1}{2} & \frac{1}{2} \end{bmatrix}; T^{-1} = \begin{bmatrix} 1 & 0 & 1 \\ \frac{-1}{2} & \frac{\sqrt{3}}{2} & 1 \\ \frac{-1}{2} & \frac{-\sqrt{3}}{2} & 1 \end{bmatrix} \tag{7}$$

Applying the mathematical relations (6) and (7) to (5), is obtain the decoupled model in the reference system $\alpha\beta\gamma$.

$$T\frac{d}{dt}\begin{bmatrix} i_{La} \\ i_{Lb} \\ i_{Lc} \end{bmatrix} = TL_{eq}^{-1}\begin{bmatrix} V_{uf}-V_{an} \\ V_{vf}-V_{bn} \\ V_{wf}-V_{cn} \end{bmatrix}$$
$$\frac{d}{dt}\begin{bmatrix} i_{L\alpha} \\ i_{L\beta} \\ i_{L\gamma} \end{bmatrix} = TL_{eq}^{-1}T^{-1}\begin{bmatrix} v_{\alpha f}-v_{\alpha n} \\ v_{\beta f}-v_{\beta n} \\ v_{\gamma f}-v_{\gamma n} \end{bmatrix} \tag{8}$$

where the equation $TL_{eq}^{-1}T^{-1}$ is given by.

$$TL_{eq}^{-1}T^{-1} = \begin{bmatrix} \frac{1}{L} & 0 & 0 \\ 0 & \frac{1}{L} & 0 \\ 0 & 0 & \frac{1}{L+3L_n} \end{bmatrix}$$

applying these mathematical relationships in (3).

$$T\frac{d}{dt}\begin{bmatrix} V_{an} \\ V_{bn} \\ V_{cn} \end{bmatrix} = T\frac{1}{C}I_{3\times3}\left[\begin{bmatrix} i_{La} \\ i_{Lb} \\ i_{Lc} \end{bmatrix} - \begin{bmatrix} i_{oa} \\ i_{ob} \\ i_{oc} \end{bmatrix}\right]$$
$$\frac{d}{dt}\begin{bmatrix} v_{\alpha n} \\ v_{\beta n} \\ v_{\gamma n} \end{bmatrix} = T\frac{1}{C}I_{3\times3}T^{-1}\begin{bmatrix} i_{L\alpha}-i_{o\alpha} \\ i_{L\beta}-i_{o\beta} \\ i_{L\gamma}-i_{o\gamma} \end{bmatrix} \tag{9}$$

The decoupled model in state variables is given by (10) and (11).

$$\frac{d}{dt}\begin{bmatrix} v_{\alpha n} \\ v_{\beta n} \\ v_{\gamma n} \end{bmatrix} = \begin{bmatrix} \frac{1}{C} & 0 & 0 \\ 0 & \frac{1}{C} & 0 \\ 0 & 0 & \frac{1}{C} \end{bmatrix}\begin{bmatrix} i_{L\alpha}-i_{o\alpha} \\ i_{L\beta}-i_{o\beta} \\ i_{L\gamma}-i_{o\gamma} \end{bmatrix} \tag{10}$$

$$\frac{d}{dt}\begin{bmatrix} i_{L\alpha} \\ i_{L\beta} \\ i_{L\gamma} \end{bmatrix} = \begin{bmatrix} \frac{1}{L} & 0 & 0 \\ 0 & \frac{1}{L} & 0 \\ 0 & 0 & \frac{1}{L+3L_n} \end{bmatrix}\begin{bmatrix} v_{\alpha f}-v_{\alpha n} \\ v_{\beta f}-v_{\beta n} \\ v_{\gamma f}-v_{\gamma n} \end{bmatrix} \tag{11}$$

The diagrams shown in Fig. 4, represent the decoupled model given by (10) and (11), where the load is represented by a linear load (R).

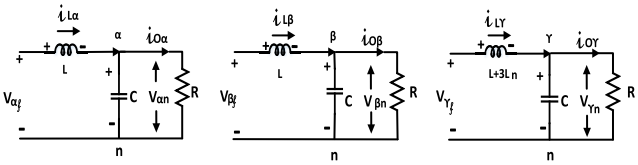

FIGURE 4. Uncoupled electrical circuit.

Considering the block diagrams of Fig.4, the mathematical relations is obtained by.

$$v_{\alpha n} = Ri_{o\alpha}, v_{\beta n} = Ri_{o\beta}, v_{\gamma n} = Ri_{o\gamma}$$

This allows to rewrite the models in state variables (10) and (11) in decoupled models for each coordinate.

$$\begin{bmatrix} \frac{di_{L\alpha}}{dt} \\ \frac{dv_{\alpha n}}{dt} \end{bmatrix} = \begin{bmatrix} 0 & -\frac{1}{L} \\ \frac{1}{C} & -\frac{1}{RC} \end{bmatrix}\begin{bmatrix} i_{L\alpha} \\ v_{\alpha n} \end{bmatrix} + \begin{bmatrix} \frac{1}{L} \\ 0 \end{bmatrix} v_{\alpha f} \tag{12}$$
$$\begin{bmatrix} \frac{di_{L\beta}}{dt} \\ \frac{dv_{\beta n}}{dt} \end{bmatrix} = \begin{bmatrix} 0 & -\frac{1}{L} \\ \frac{1}{C} & -\frac{1}{RC} \end{bmatrix}\begin{bmatrix} i_{L\beta} \\ v_{\beta n} \end{bmatrix} + \begin{bmatrix} \frac{1}{L} \\ 0 \end{bmatrix} v_{\beta f} \tag{13}$$
$$\begin{bmatrix} \frac{di_{L\gamma}}{dt} \\ \frac{dv_{\gamma n}}{dt} \end{bmatrix} = \begin{bmatrix} 0 & \frac{-1}{L+3L_n} \\ \frac{1}{C} & -\frac{1}{RC} \end{bmatrix}\begin{bmatrix} i_{L\gamma} \\ v_{\gamma n} \end{bmatrix} + \begin{bmatrix} \frac{1}{L+3L_n} \\ 0 \end{bmatrix} v_{\gamma f} \tag{14}$$

The models in state variables for α and β axes are equal as can be seen in expressions (12) and (13). The model for the γ axis expression (14) presents the inductance effect of the neutral wire.

The following subsection presents the analysis by transfer function.

B. ANALYSIS BY TRANSFER FUNCTION

Let us consider only the component □ of the inverter model, which is represented by equation (12). The block diagram of this model is shown in Fig. 5. Note that this model also applies to coordinate β.

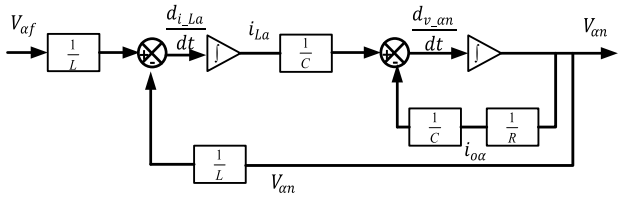

FIGURE 5. Block diagram of the α axis.

This diagram is the most important in this work, since it is used to obtain the transfer functions that allow the current and voltage loop controllers design.

Applying block algebra to the diagram in the Fig. 5, the transfer function that relates the output voltage $v_{\alpha n}$ and the current signal $i_{L\alpha}$ is obtained by.

$$G_1(s) = \frac{v_{\alpha n}(s)}{i_{L\alpha}(s)} = \frac{R}{sCR+1} \tag{15}$$

The transfer function that relates the output voltage $v_{\alpha n}$ and the input signal $v_{\alpha f}$ is given by (16).

$$G_2(s) = \frac{v_{\alpha n}(s)}{v_{\alpha f}(s)} = \frac{R}{s^2LCR+sL+R} \tag{16}$$

Finally, the transfer function that relates the current signal $i_{L\alpha}$ and the input voltage $v_{\alpha f}$ is given by (17).

$$G_3(s) = \frac{i_{L\alpha}(s)}{v_{\alpha f}(s)} = \frac{sCR+1}{s^2LCR+sL+R} \tag{17}$$

Note that relationships are fulfilled.

$$G_2(s) = G_3(s)\,G_1(s) = \frac{i_{L\alpha}(s)}{v_{\alpha f}(s)}\frac{v_{\alpha n}(s)}{i_{L\alpha}(s)} = \frac{v_{\alpha n}(s)}{v_{\alpha f}(s)}$$

Taking into account, that the average current in the inverter output filter inductor and inverter output voltage must be regulated, a master-slave control scheme is used. The slave loop controller allows to regulate the inductor current and the master loop controller allows regulates the inverter output voltage. The control scheme is shown in Fig. 6, where $G_v(s)$ and $G_i(s)$ are the transfer functions representing the voltage and current loop controllers, respectively; $v_{\alpha r}(s)$ is the reference signal for phase α, $G_1(s)$ and $G_3(s)$ are the transfer functions obtained in (15) and (17).

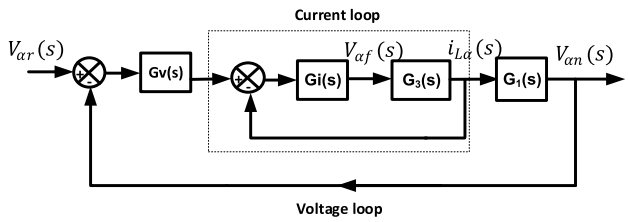

FIGURE 6. Master-slave control scheme for the inverter.

The transfer functions for γ axis is obtained by following the same steps that are carried out for the α axis. The transfer functions of γ axis are given by the equations (18)-(20). In obtaining these equations, the model presented in state variables (14) is used.

$$G_4(s) = \frac{v_{\gamma n}(s)}{i_{L\gamma}(s)} = \frac{R}{sCR+1} \tag{18}$$

$$G_5(s) = \frac{v_{\gamma n}(s)}{v_{\gamma f}(s)} = \frac{R}{s^2CR\,(L+3L_n)+s\,(L+3L_n)+R} \tag{19}$$

$$G_6(s) = \frac{i_{L\gamma}(s)}{v_{\gamma f}(s)} = \frac{sCR+1}{s^2CR\,(L+3L_n)+s\,(L+3L_n)+R} \tag{20}$$

The following subsection presents the inverter output filter design. The parameters of the inverter output filter are calculated below.

C. INVERTER OUTPUT FILTER DESIGN

The calculation of the four-wire inverter output filter is obtained considering that each phase of the three-phase inverter with respect to the neutral is equivalent to a single-phase inverter. Another factor that is considered for its design is its crossover frequency for which it is recommended that it be between 15 harmonic and 17 harmonic; in order to provide greater disturbance rejection. Considering this, the equivalent circuit for each phase that allows to determine the filter transfer function is presented in Fig. 7.

Applying the Kirchhoff law of voltages and Laplace transform, the transfer function is determined by (21).

$$\frac{V_o(s)}{V_i(s)} = \frac{1}{s^2CL+1} \tag{21}$$

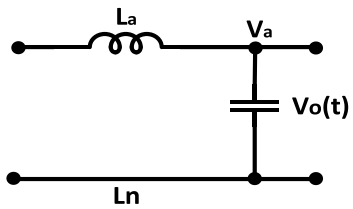

FIGURE 7. Equivalent circuit for calculating the inverter output filter.

from which it is obtained (22)

$$\omega_n = \sqrt{\frac{1}{CL}} \tag{22}$$

Considering an attenuation of -3dB and a crossing frequency *fn* of 934 Hz that is between the 15th harmonic and the 17th harmonic and using the expression (23), the following values of the filter parameters are obtained by.

$$f_n = \frac{1}{2\pi\sqrt{LC}} \tag{23}$$

where, an inductance with a value L =880μH is proposed, and the capacitor value is calculated from the expression (23); being its value C= 33μF.

In Table 1, the main parameters and their inverter values are shown.

TABLE 1. Parameters of the inverter.

Parameter	Value
Inverter nominal power (P)	3kW
DC_LINK voltage (v_{DC})	390V
Inverter output voltage (V_o)	110V
Inverter output frequency (f_o)	60Hz
Inverter output inductance (L)	880µH
Inverter output capacitor (C)	33µF
Load resistance	12Ω
Sample frequency	15kHz
Inverter switching frequency (f_s)	15 kHz

The next section presents the methodology used to control scheme design presented in Fig. 6. This method allows the current controllers design (slave loop) and the voltage loop (master loop).

III. CONTROL SCHEME DESIGN

The proposed methodology for the master and slave loop controllers design is simple and direct. This methodology is based on the frequency analysis [25]. In this work, a controller with proportional-integral (PI) structure is proposed.

$$G_c(s) = k_p + k_i\frac{1}{s}$$

Considering the inverter cutoff frequency, the cutoff frequency ω_{co} is selected. Using this condition and considering a phase margin Ph_m between 50° and 90° it is possible to

obtain the controllers gains. In general, the steps to follow in the design are the following.

1) The open-loop transfer function $G_{ol}(s)$ of the controller-plant set is obtained.
2) The crossover frequency $\omega_{co}$and the phase margin Ph_m are selected.
3) The open-loop transfer function at the crossing frequency ω_{co} is evaluated and considering the conditions of magnitude and phase, the gains of the controller are obtained.

On the other hand, once this controller is designed, a coordinate transformation method is applied to obtain a new controller named proportional controller plus a generalized integrator (P+GI). This method is summarized as follows: once the PI controller is designed in direct current (dc), a coordinate transformation is applied to the integral control action, which allows obtaining a generalized integrator at the system's operating frequency "60Hz" and therefore a controller in (ac).

This new controller is integrated a proportional controller plus a generalized integrator (P+GI). The transformation allows obtaining a new controller in a synchronous or *ac* reference system from a controller in a stationary or *dc* reference system. The controller designed in *ac* presents a better performance, minimizing the errors in steady state of amplitude and phase of the inverter voltage and current signals; besides improving the disturbances rejection to the converter operation frequency [22].

The following subsection presents the PI controller design in dc.

A. PI CONTROLLER

The open loop transfer function $G_{ol}(s)$ is represented by expression (24), where a feedback control scheme is considered. $G(s)$, is the controller transfer function of process or plant and $G_c(s)$ is the controller transfer function.

$$G_{ol}(s) = \left(k_p + \frac{k_i}{s}\right) \cdot G(s) = k_p \cdot (s + \beta)\, G_n(s) \tag{24}$$

where $\beta = \frac{k_i}{k_p}$ and $G_n(s) = \frac{G(s)}{s}$.

The open-loop sinusoidal transfer function $G_{ol}(j\omega)$ is given by (25).

$$G_{ol}(j\omega) = k_p\,(j\omega + \beta)\, G_n(j\omega) \tag{25}$$

The open-loop transfer function when evaluated at the crossover frequency ω_{co} has gain one, as shown in expression (26).

$$k_p\,|j\omega_{co} + \beta|\,|G_n(j\omega_{co})| = 1 \tag{26}$$

Performing some algebraic operations, it gets the relation (27).

$$k_p = \frac{1}{|G_n(j\omega_{co})|\sqrt{\beta^2 + \omega_{co}^2}} \tag{27}$$

The next step is to propose a phase margin Ph_m between 50° y 90°. From this condition, expression (28) is obtained by.

$$-180^0 + Ph_m = (j\omega_{co} + \beta) + \sphericalangle\,(G_n(j\omega_{co}) \tag{28}$$

Performing some algebraic operations, a second condition is obtained, that is shown by (29).

$$\beta = \frac{\omega_{co}}{tan\left(Ph_m - 180^0 - \sphericalangle\,(G_n(j\omega_{co})\right)} \tag{29}$$

The gains k_p *and* y k_i are obtained by solving equations (27) and (29).

The following subsection presents the P+GI controller design by coordinate transformation method.

B. P+GI CONTROLLER DESIGN METHOD BY COORDINATE TRANSFORMATION

The objective of the integral part of the PI controller is to reduce the steady state error of the system to zero, $e_{ss} = 0$ when the input signal is a step type, so it is said that they are designed in dc. However, when the reference signal is sinusoidal, a new compensator that presents a good performance for this type of signal must be designed. With this criterion, a proportional plus generalized integrators controller is proposed in this work. The controller is designed so that the inverter works both at the system operating frequency and at the harmonics frequency that occur when supplying local load; linear and nonlinear in this operation mode. The objective of a (P+GI) controller is to achieve a phase and zero magnitude error in *ac* systems [22]. This compensator is obtained based on the PI controller previously designed in *dc* and applying the *dc-ac* coordinate transformation shown in expression (30).

$$G_{AC}(s) = G_{DC} \cdot \left(\frac{s^2 + \omega_o^2}{2s}\right) \tag{30}$$

where $G_{DC}(s)$ and $G_{AC}(s)$ are the control schemes in *dc* and *ac* respectively, ω_o is the fundamental system operating frequency and the complex variable is replaced by, $\frac{s^2+\omega_o^2}{2s}$. In other works developed, this strategy is solved by an approximation using the transfer function of a low-pass filter, as shown in expression (31).

$$G_{DC}(s) = k_p + k_i \frac{\omega_B}{s + \omega_B} \tag{31}$$

Therefore, the *ac* compensator, which we will call the P+GI controller, is represented as shown in the expression (32).

$$G_{AC}(s) = k_p + k_i \frac{2\omega_B s}{s^2 + 2\omega_B s + \omega_o^2} \tag{32}$$

ω_B represent the lowest crossover frequency of the dc transfer function, k_p and k_i are the gains of the PI controller previously obtained [10].

1) CURRENT AND VOLTAGE LOOP CONTROLLER α AXIS

The design of the slave loop is based on the controller design methodology presented in section III, as well as in the block diagram presented in Fig. 6. Particularly in this section the current loop controller design is described. The frequency at which the crossover gain of the current or slave loop occurs is selected as $f_{co_e} = 1.5$ kHz, which is 10 times less than the switching frequency $f_s = 15$ kHz, and the phase margin Ph_{m_e} is selected from 60^0. The sub-index _s indicates that the data is for the design of the slave loop.

The open loop transfer function is given by (33).

$$G_{ol_s}(s) = k_{p_s}\left(s + \frac{k_{i_s}}{k_{p_s}}\right)\frac{G_3(s)}{s} = k_{p_s}(s+\beta_s)\frac{RCs+1}{s\left(s^2LCR + sL + R\right)} \quad (33)$$

When replacing in the expressions (26)-(29), the values of the proportional and integral gains of the slave loop controller are obtained.

$$k_{p_s} = 4.18 \; and \; k_{i_s} = 31508 \quad (34)$$

On the other hand, the P+GI controller is obtained directly from the expression (32), with the gains k_{p_s} and k_{i_s} given in (34), $\omega_B = 0.2$ rad / s and the fundamental frequency $\omega_0 = 2\pi \cdot 60$ rad/s.

The Bode diagrams of the open loop transfer functions of the PI and P+GI controllers are shown in Fig. 8. The phase margin for the PI controller is 60^0 to 1.5 kHz according to the controller design proposal. The phase margin for the P+GI controller is of 66.3^0 to 1.45 kHz.

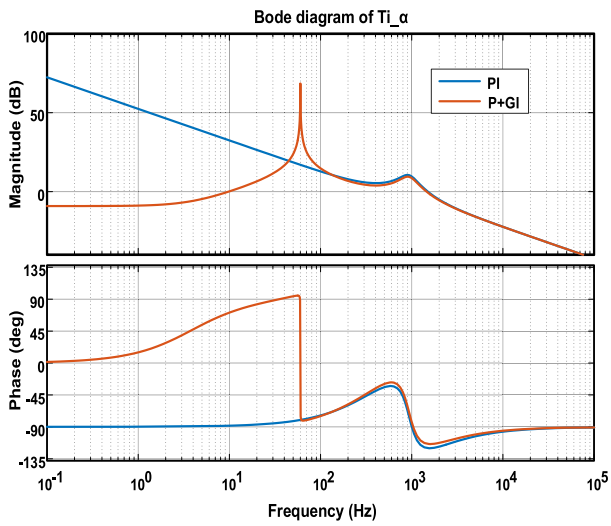

FIGURE 8. Bode diagram of PI vs P+GI controller for slave loop α axis.

The main difference between the two control proposals is the low frequency behavior of the P+GI controller, where it is observed that at 60 Hz there is a high gain. This gain is due to the coordinate transformation of the integral action that is obtained from the PI controller design in the *dc*. This feature allows a better tracking of the command and improves the disturbances rejection at the inverter operating frequency.

The controller for the master loop is implemented following the same design methodology as the slave loop. This control establishes the reference that the slave controller should follow. The open loop transfer function $G_{ol_m}(s)$ for the voltage loop design is given by the expression (35) where the sub-index m indicates master loop. The open loop transfer function is be obtained from the diagram of Fig.6.

$$G_{ol_m}(s) = G_v(s)\frac{G_i(s)\,G_3(s)}{1 + G_i(s)\,G_3(s)}G_1(s) \quad (35)$$

where the current controller transfer function $G_i(s)$ is designed in sub-section III.B and $\frac{G_i(s)G_3(s)}{1+G_i(s)G_3(s)}$ is the closed-loop transfer function of the slave loop and is given by

$$\frac{G_i(s)\,G_3(s)}{1 + G_i(s)\,G_3(s)} = \frac{0.019s^2+199.9s+37810}{1.38\times10^{-4}s^4+1.35\times10^{-6}s^3+0.013s^2+41.14s+35510}$$

The transfer function of the voltage control scheme $G_v(s)$ is selected again as a PI control.

$$G_v(s) = k_{p_m} + k_{i_m}\frac{1}{s} = k_{p_m}\left(\frac{s+\beta_m}{s}\right)$$

where the subscript m indicates master loop, when solving the expressions (27) and (29) and considering the crossover frequency of the master or voltage loop as $f_{co_m} = 700$ Hz; and the phase margin Ph_{m_m} of 90^0 the proportional and integral gain values of the controller are obtained in (36). The crossover frequency of the voltage loop was chosen with a value close to half the current loop crossover frequency, its choice is justified considering that the overall stability of the system is not affected, obtaining a phase of 90°. Furthermore, this bandwidth allows a greater number of generalized integrators to be designed. This is justified in Fig 12, where generalized integrators were added to the grid operating frequency and to the frequency of the 3rd and 5th harmonic, which allows to have a greater system disturbances rejection

$$k_{p_m} = 0.21, \; and k_{i_m} = 336.1 \quad (36)$$

The P+GI controller obtained by the *dc-ac* transformation method is calculated directly from the expression (29), with the gains k_{p_m} and k_{i_m} given in (36), $\omega_B = 0.2$ rad / s and the fundamental frequency given by $\omega_0 = 2\pi \cdot 60$ rad/s.

The Bode diagrams of the open-loop transfer functions of the PI and P+GI controllers are shown by Fig. 9.

The phase and gain margins of the PI controller are 90° to 701 Hz and 17.9 dB to 2.8 KHz. The phase and gain margin of the P+GI controller are 94.2° to 666 Hz and 18.9 dB to 3.06 KHz.

2) CURRENT AND VOLTAGE LOOP CONTROLLER FOR γ AXIS

Particularly, inverter coordinate γ presents the effect of the neutral wire given by expression (14) so that in this section

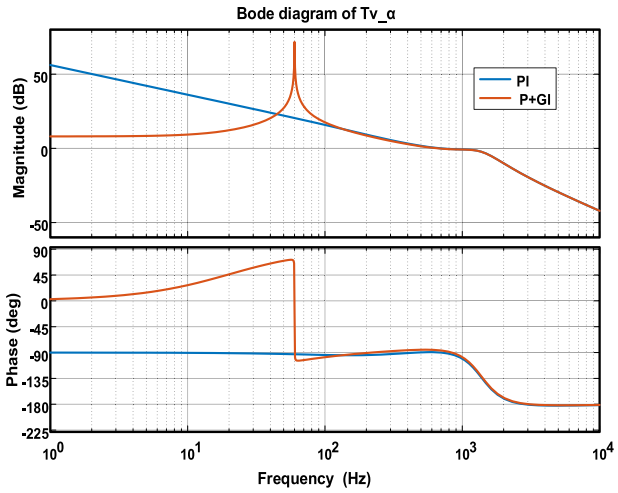

FIGURE 9. Bode diagram of controller PI vs P+GI for master loop α axis.

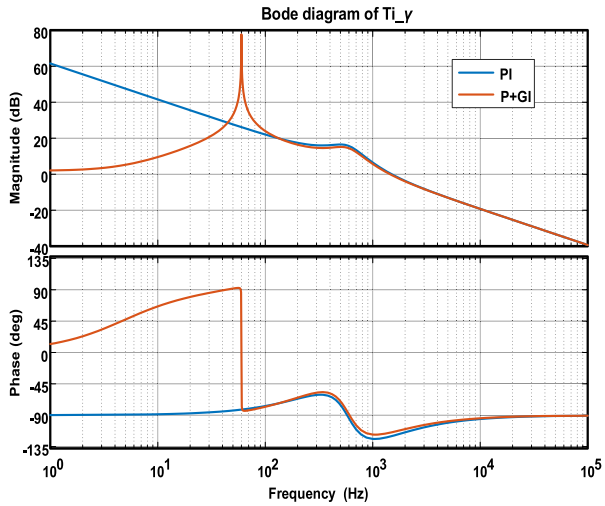

FIGURE 10. Current loop Bode diagram. Axis γ.

the control schemes design for this phase is carried out. The procedure performed to obtain the controllers of α axis is applied again to obtain the gains of the controllers for γ axis. Remember that the transfer functions for this coordinates are given by expressions (18)-(20). When applying the same methodology presented in subsections III.A and III.B, the proportional and integral gains for the slave or current loop and for the master or voltage loop are given by (37).

$$k_{p_s} = 4.18, \quad k_{i_s} = 31508$$
$$k_{p_m} = 0.21, \quad k_{i_m} = 336.1 \tag{37}$$

where again the sub-indices s and m represent slave loop and master loop. The current and voltage Bode diagrams for the PI and P+GI control schemes are shown in Figs. 10 and 11. The design conditions are the same as those used for α axis, that is, for the slave loop the crossover gain is $f_{co_s} = 1.5$ kHz and the phase margin Ph_{m_s} is 60^0. The crossover frequency and the phase margin of the master loop are $f_{co_m} = 700$ Hz and $Ph_{m_m} = 90^0$ respectively.

In Fig. 10, the Bode diagram of current loop presents a phase margin for the PI controller from 60° to 1.5 kHz, satisfying the design conditions, while for the P+GI controller it is from 64.9° to 1.45 kHz. In Fig. 11, the voltage loop Bode diagram presents a phase margin for the PI controller of 90° to 700 Hz and a phase margin of 94.6° to 673 Hz for the P+GI controller. In both cases the graphs of Figs. 10 and 11 show behavior similar to the Bode diagrams obtained for γ axis.

Fig. 12, shows the open-loop Bode diagram with the controller implementation (P+GI), considering generalized integrators to the grid frequency and load harmonics frequency (3rd and 5th); as well as with the PI controller implementation. Presenting, the following stability margins: phase margin for the PI controller from 90 ° to 700 Hz and a phase margin from 79.5 ° to 830 Hz for the P+GI controller.

It is important to mention that in the P+GI's controllers design at the 3rd and 5th harmonics frequency, the same gains of the PI controller and the structure (32) were used,

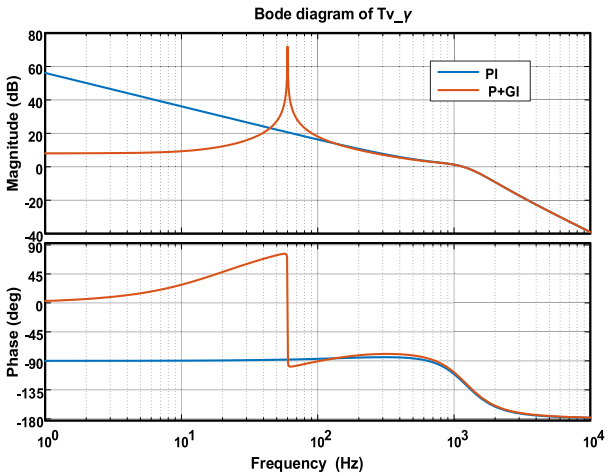

FIGURE 11. Voltage loop Bode diagram Axis γ.

modifying only the frequency ω_o at which the harmonics occur.

The following section presents the results obtained through the inverter operation simulations in island mode and with the implementation of control schemes designed in the previous section. These results are obtained by feeding linear and non-linear load.

IV. SIMULATION RESULTS

The digital simulations reported in this paper are obtained using two controller combinations:

1) **Scheme 1**. PI controller in the slave loop and PI controller in the master loop.
2) **Scheme 2**. PI controller in the slave loop and P+GI controller in the master loop.

These combinations present a better dynamic performance unlike when the P+GI controller was used in the slave loop (current loop). This is justified because, in inverter island mode operation is responsible for regulating the output

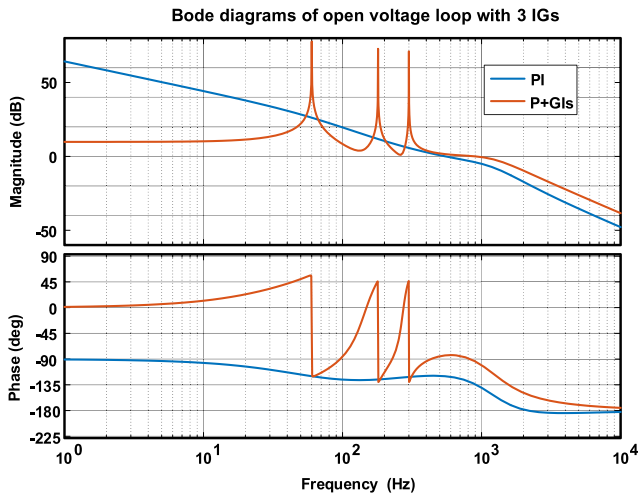

FIGURE 12. Voltage loop Bode diagram Axis γ, with three generalized integrators added to the harmonic's frequency (3rd and 5th).

voltage and the waveform of the current is determined by the type of load to be fed. Particularly, this better behavior occurs when non-linear loads are fed.

The control strategies designed were implemented in MATLAB/Simulink and the inverter was simulated in the PowerSim computer package. The data communication between both platforms was carried out through the Sim-Coupler tool of PSIM^{TM}. In digital simulations, two tests are considered:

1) Test 1 Linear load R = 12 Ω balanced in all three phases and with an imbalance in one of the phases
2) Test 2. Non-linear load in the three phases, the load consists of a rectifier diode bridge and a filter with a capacitance of 180 μF and a resistance R = 12 Ω.

A. TEST 1. LINEAR LOAD (R), SCHEME 1

Two test were carried out in the first, a balanced load of 12 Ω was connected to the inverter output. In a second test an imbalanced load was connected, particularly between phases *a* and *b* and the neutral wire was connected a load of 12 Ω, while between phase c and neutral wire a load of 8 Ω, it was connected.

In the Fig. 13 the output voltage signals versus their reference signals is obtained using scheme 1. In this Fig. It is observed that the output voltage signals of the three phases present a setpoint tracking error. However, the voltage signals have: adequate waveforms, frequency and amplitude.

The THD presented by these voltage signals is 0.9%. In Figs. 14 (a) and (b), the graphs of the three phases current signals are observed when the inverter supplies balanced and unbalanced linear loads, respectively.

Particularly in the Fig.14(b) an increase in the current of phase *c* is observed due to the higher load that was connected between the phase c and the neutral wire, however the output voltages of the three phases maintains its waveforms of amplitude and frequency, respectively.

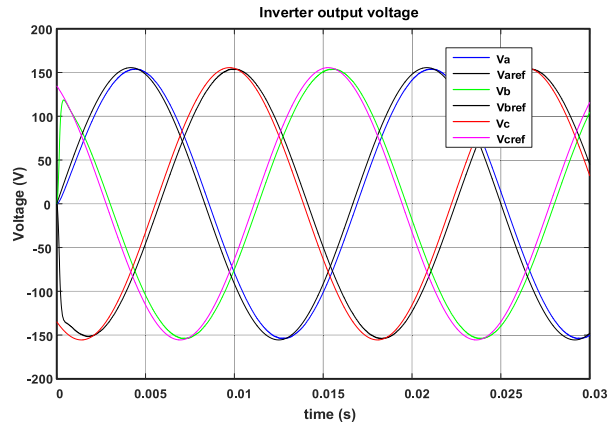

FIGURE 13. Waveforms of voltage signals, scheme 1.

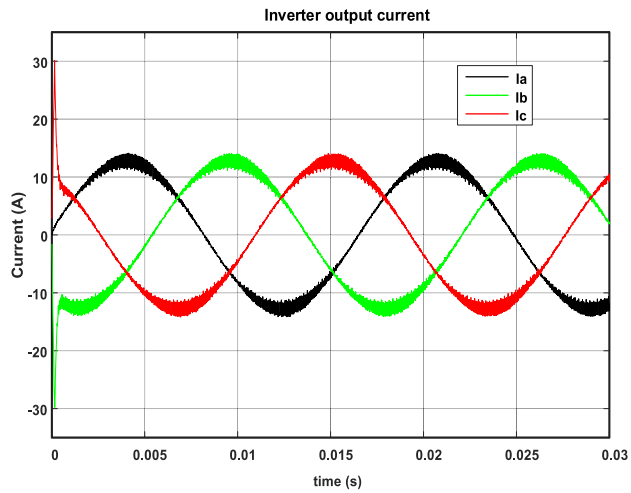

(a)

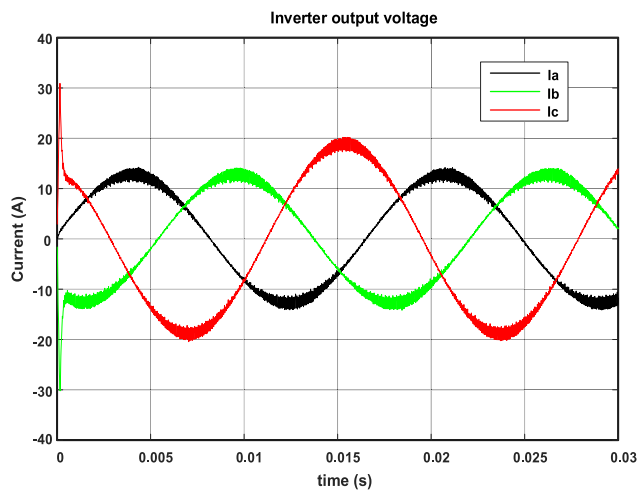

(b)

FIGURE 14. (a). Waveforms of current signals, scheme 1 with balanced load. (b). Waveforms of current signals, scheme 1 with unbalanced load.

B. TEST 1. LINEAR LOAD (R), CONTROL SCHEME 2

On the other hand, when scheme 2 is implemented, the tracking error is minimized compared to the results obtained with the implementation of scheme 1, this can be seen in Figs. 15.

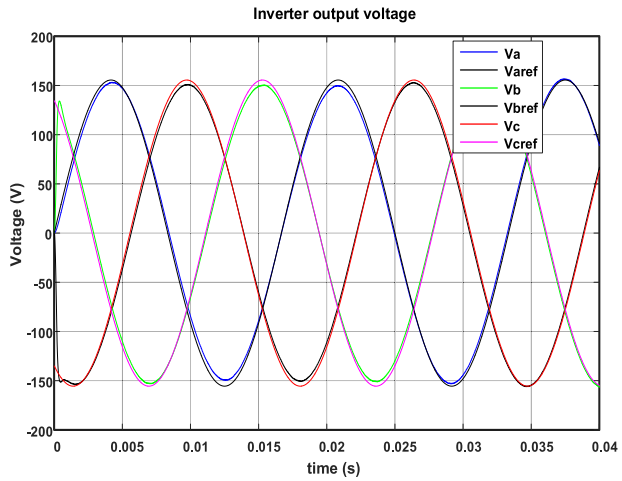

FIGURE 15. Waveforms of voltage signals, scheme 2.

Also, in Fig. 16 (a), (b) and (c), the graphs of the currents of the three phases are presented when the inverter feeds balanced and unbalanced linear loads respectively. In 16 (b) an increase in the current of phase c is observed due to the greater load that was connected between phase c and the neutral wire, however, the output voltages of the three phases maintain their waveforms of amplitude and frequency respectively. Particularly in Fig 16 (c), it is observed that when the loads fed by the inverter are balanced, the current through the neutral wire presents a value close to zero. This behavior is similar when control schemes 1 and 2 are used.

C. TEST 2. NON-LINEAR LOAD, CONTROL SCHEME 1

In a second test, a balanced non-linear load it is connected at the inverter output with the following characteristics: a Diode Bridge, a 12 Ω resistor in parallel with a 220 μF capacitor. This test is very important, since it allows evaluating the inverter performance with the implementation of the P + GI controller versus the PI controller.

Figs. 17 and 18, show the voltage waveforms and inverter output current when scheme 1 is implemented. In addition, in Figs. 20 and 21 these same signals are presented when scheme 2 is implemented.

Particularly, in the Fig. 17, it is observed that the output voltage signals present a non-sinusoidal waveform, this due to the characteristics of the non-linear load that causes a total harmonic distortion of this signal (THDv=10.7 %). Also, their reference signals are out of phase; and the peak-to-peak output voltage is greater than their respective reference signals. In Fig. 18, is shows the current signals of each phase, which have a non-sinusoidal waveform caused by non-linear load. This causes the inverter current waves to have an amplitude of about ± 20 A peak-to-peak. These responses are obtained when implementing control scheme 1.

In Fig. 19, the phase A and neutral wire waveforms are presented when the inverter supplies non-linear load. In this test, the phase currents present an imbalance of approximately 6 A, considering that the current amplitude when the inverter supplies linear load is approximately 12 A peak to peak and with non-linear load it is 18 A peak to peak.

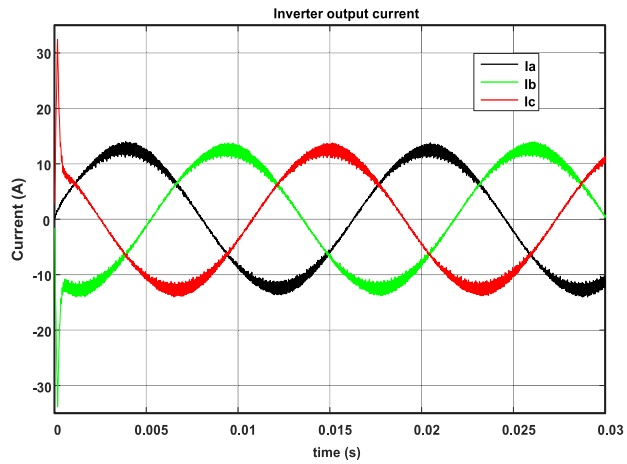

(a)

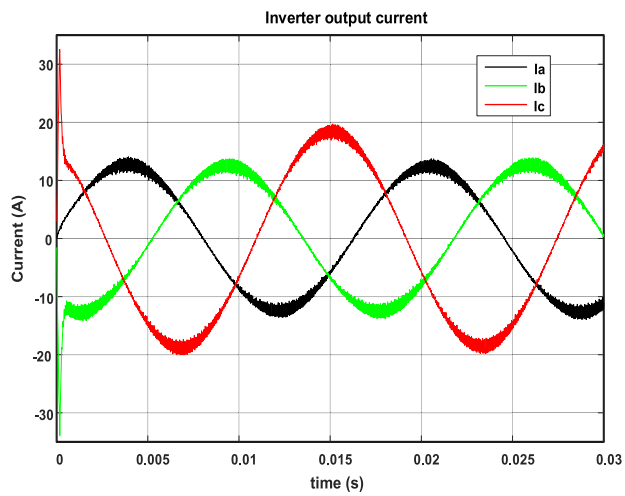

(b)

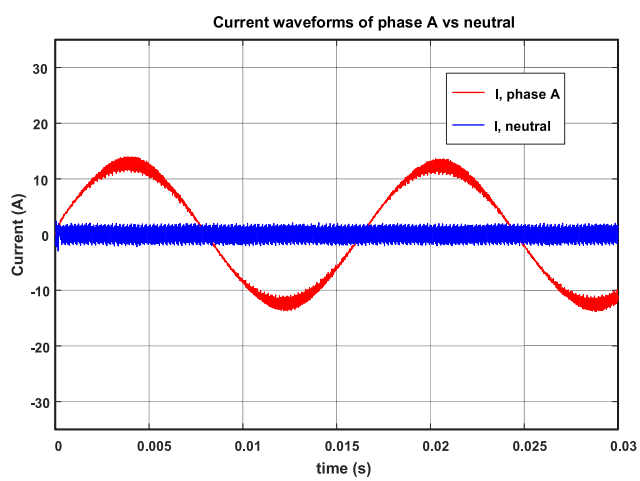

(c)

FIGURE 16. (a). Waveforms of current signals, scheme 2 with balanced load. (b). Waveforms of current signals, scheme 2 with unbalanced load. (c). Waveforms of current signals, scheme 1 and 2 with balanced load.

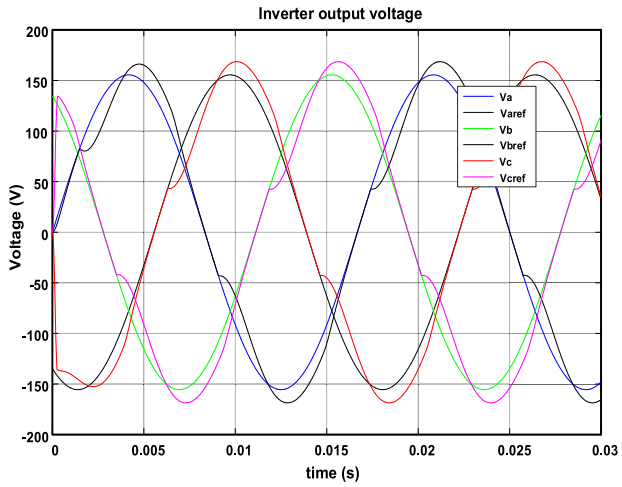

FIGURE 17. Waveforms of voltage signals, scheme 1, feeding non-linear load.

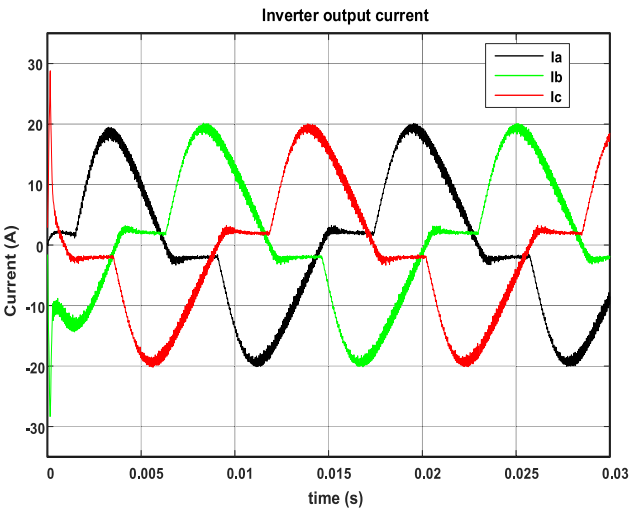

FIGURE 18. Waveforms of current signals, scheme 1, feeding non-linear load.

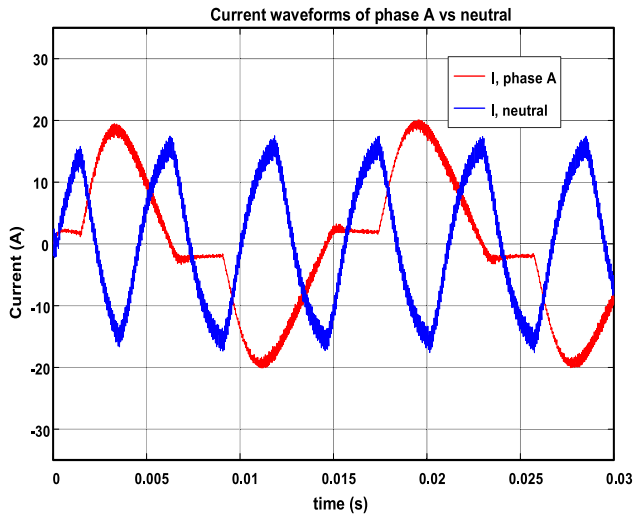

FIGURE 19. Waveforms of phase A and neutral wire.

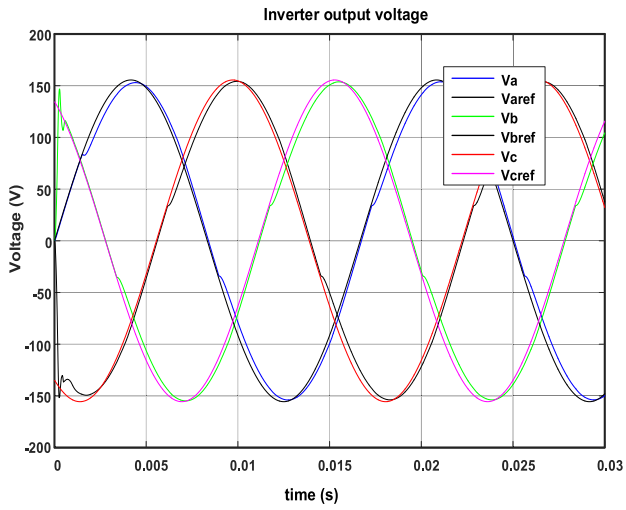

FIGURE 20. Waveforms of voltage signals, scheme 2, feeding non-linear load.

Therefore, the amplitude of the current flowing through the neutral wire is approximately 18 A peak to peak as shown in the graph.

In Fig. 20, a lower total harmonic distortion of the voltage signal is observed (THDv = 5.4 %) compared to the results obtained with control scheme 1 (THDv = 12.8 %). In this test, the offset between the reference signals and the inverter output voltages is reduced, achieving better setpoint tracking. Furthermore, the amplitudes of both signals are similar.

In Fig. 21, the current signals of each phase are shown, which have a non-sinusoidal waveform caused by the non-linear load feeding the inverter. However, compared to the previous test, the currents have a greater amplitude with a value of 21 A peak to peak. These responses are obtained by implementing control scheme 2.

In Fig. 22, the phase A and neutral wire waveforms are presented when the inverter supplies non-linear load. In this test the phase currents present an imbalance of approximately 5 A, considering that the current amplitude when the inverter supplies linear load is approximately 15 A peak to peak and with non-linear load it is 20 A peak to peak. Therefore, the amplitude of the current flowing through the neutral wire is approximately 15 A peak to peak as shown in the graph. This shows that with control scheme 2, the sum of the total current flowing through the neutral is less than when control scheme 1 is used.

On the other hand, in Fig. 23 the waveforms of voltage signals that were obtained with the implementation of generalized integrators at the load harmonics frequency (3rd and 5th) are presented. In this figure there is less distortion in the inverter output voltage signal, as well as a better setpoint tracking, this compared with the results obtained in Fig. 20; which confirms that the controller designed under scheme

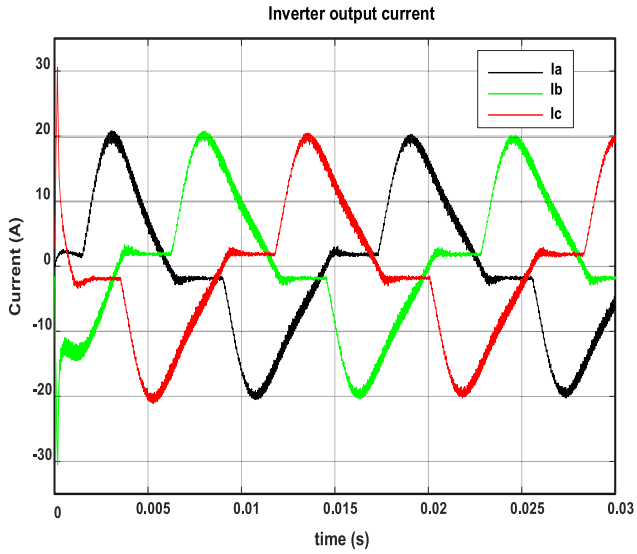

FIGURE 21. Waveforms of the current signals, scheme 2, feeding non-linear load.3

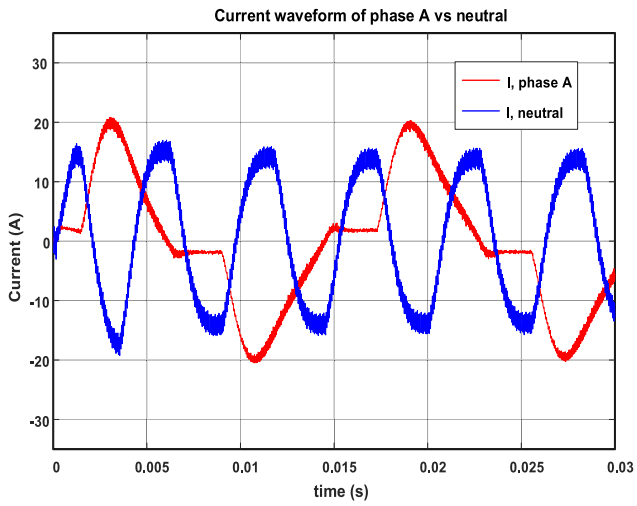

FIGURE 22. Waveforms of phase A and neutral wire.

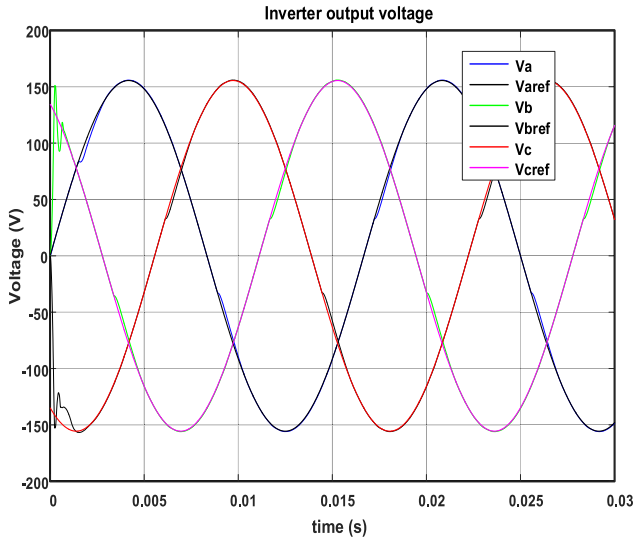

FIGURE 23. Waveforms of voltage signals, scheme 2, feeding non-linear load with three generalized integrators.

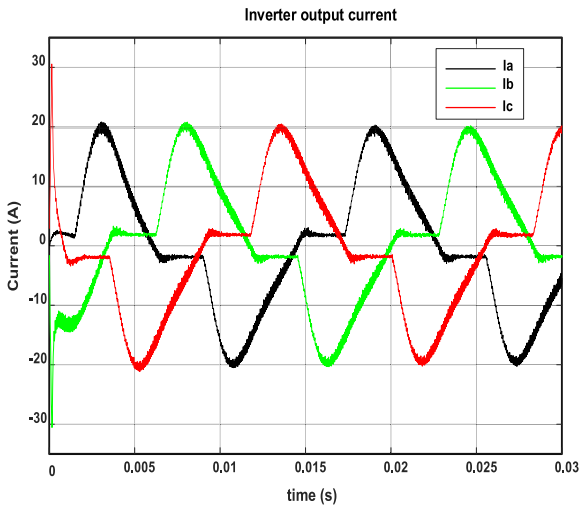

FIGURE 24. Waveforms of the current signals, scheme 2, feeding non-linear load with three generalized integrators.

2 presents a good performance. Also, Fig. 24 shows the waveform of inverter output current signals.

Finally, simulations are presented for changes in load and unbalance of their lines that allow observing the inverter performance and the implemented controllers.

In Fig. 25, the waveform of voltage and current supplied by the inverter are presented when a load change occurs. In this figure it can be seen how during the load change transition, the output voltage is maintained at its nominal value and the current in the neutral wire has a value close to zero.

In Fig. 26, inverter waveforms are presented when a load imbalance occurs; observing that in the neutral wire circulates a current with an inverter operation nominal value, maintaining in equilibrium the system and therefore a good performance.

In Fig. 27 the harmonic spectrum of the inverter voltage signals is presented, which were obtained with the implementation of a PI controller in dc, a P+GI controller that was obtained by applying coordinate transformation and which allowed obtaining an integrator generalized to the system operating frequency. In addition, a P + 3GI controller, characterized by having three generalized integrators: for the system operating frequency and the frequency of the third and fifth harmonic of the non-linear load that is supplied.

In the next section, the results analysis discussion previously obtained through simulations are presented.

V. RESULTS DISCUSSION

In the tests carried out, the advantages of the methodology developed in this work are observed, particularly in

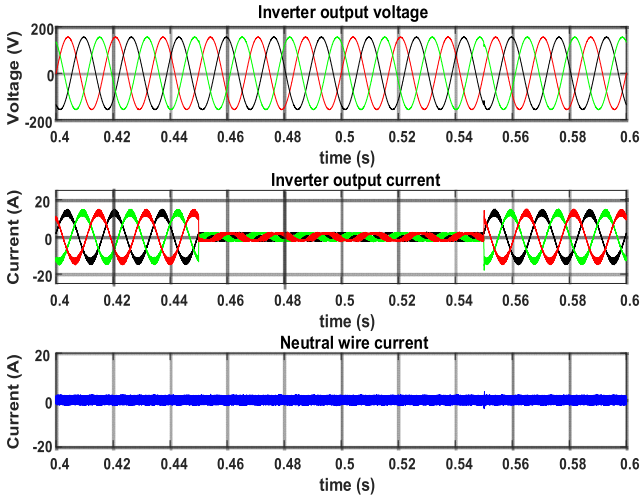

FIGURE 25. Waveform detail of voltage and current when load changes occur.

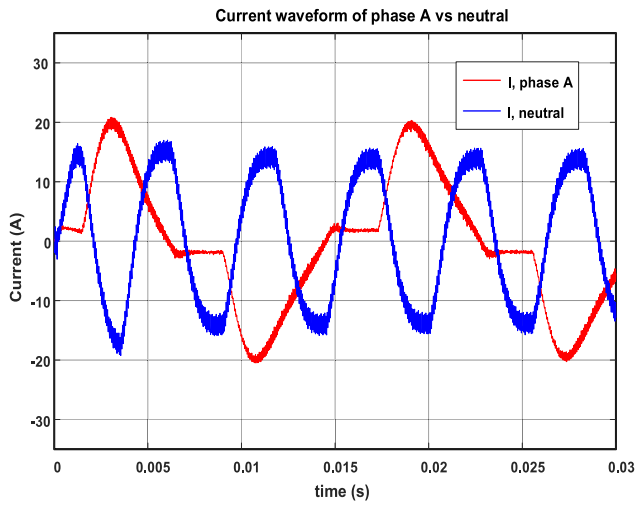

FIGURE 26. Waveform detail of voltage and current when load imbalance occurs.

the results obtained with the control scheme design by the coordinate transformation method in *ac* (P+GI), over the control schemes classics (PI) designed in *dc*. In the simulations carried out with the PI controller implementation in the current and voltage loop, feeding the linear load (Fig. 13), a low performance of the controller is observed, that is, with this implementation the inverter has a non-zero steady-state error (eee $\neq 0$). That is, there is a reference signal tracking error that is imposed on the inverter, however, the currents are distributed in a balanced way with a current value of 12.96 A peak to peak; value that is proportional to the linear nominal load of 12 Ω (Fig. (14 (a)). When a load imbalance occurs in the inverter phase c from 12 Ω to 8 Ω, an increase in the current of this phase occurs, going from 12.96A to 19.44 A, which is observed (Fig. 14 (b)).

On the other hand, when a PI controller is implemented in the current loop and a P + GI controller in the voltage

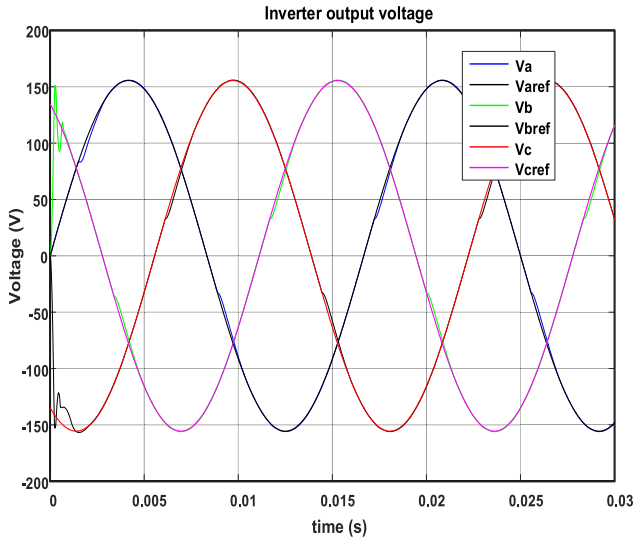

FIGURE 27. Harmonic spectrum of inverter voltage signals.

loop (Fig. 15), a better inverter performance is observed, that is, the error has a value close to zero (eee ≈ 0) producing a better set point tracking. This is presented by the action of the generalized integrator that occurs at the system reference signal frequency. For this test, the behavior of the currents is similar to that presented in the previous case (Fig. 16 (a)) and (Fig. 16 (b)).

In the simulations performed with the PI controller implementation in the current loop and the voltage loop and feeding non-linear load (Fig. 17), a low controller performance is observed a poor inverter set point tracking, that is, the eee > 0. Also, there is an increase in the amplitude of the inverter output voltage signal with a value of 168 V peak-to-peak with respect to the reference voltage that is 155.5 V. In this test, it is clearly seen that the inverter performance decreases by compared to that presented when feeding a linear load, that is, the eee is greater. However, the currents are evenly distributed and their waveform is characteristic of a non-linear load (Fig. (14 (a)).

Similarly, to the linear load test, when PI controller is implemented a in the current loop and a P+GI controller in the inverter voltage loop, feeding a non-linear load (Fig. 20); a better inverter performance is presented; observing a better setpoint tracking, eee=0. This is presented by the action of the generalized integrator that is designed at the system reference signal frequency. In this case the behavior of the currents is similar to that presented in the previous case (Fig. 21).

In conclusion, presenting quantitative data, with the PI controller implementation in the current loop and a P+GI controller in the voltage loop the converter reduces the total harmonic distortion (THDv) of the voltage signal from 10.7 % to 5.4 %.

Taking into account that the value of THDv allowed by the normative that must be less than 5 %, generalized integra-

tors are added to the harmonic frequency (3rd and 5th) as shown in (Fig. 12); allowing to reduce the THDv of 5.4 % to 2.2 % (Fig. 23). These tests were performed with a non-linear load with a value equivalent to the nominal value; which shows that this presents a good performance. Also, with the implementation of a greater number of generalized integrators, better setpoint tracking is achieved as shown in Fig. 23.

Finally, Fig. 25 and 26, allow to observe a good inverter performance in case of load changes and unbalance of any of the phases of this. In this Figs, it is observed that when the load changes from 0 A to nominal current values of 12.96 A peak-to-peak, the inverter output voltage maintains its waveform, amplitude (155.5 V) and frequency (60 Hz).

VI. CONCLUSION

This paper is present the modeling for a four-wire three-phase inverter, the method for obtaining the transfer functions and in the controllers design obtained by this method. In particular, a current loop and a voltage loop are considered in the inverter model; which allows to clearly obtain the transfer functions of both loops. The main advantage of this proposal is that when the kp and ki gains are obtained through the Bode diagrams, is can obtain generalized integrators; applying the coordinate transformation method to the integral gain that was obtained by the design of the PI controller in direct current (dc). This allows obtaining a new controller that in this work was defined as a proportional control plus generalized integrator (P+GI). This new controller was specially designed for the voltage loop (master controller), considering that in inverter island mode operation the objective is to maintain the waveform, amplitude and frequency of the voltage signal. Therefore, a PI controller was used in the current loop (slave controller).

To evaluate the performance of the inverter with the implementation of the designed controllers: PI controller, P + GI, tests were performed with linear and non-linear load, as well as with load changes. Particularly, with the PI controller implementation, is observed that this present setpoint tracking error greater than zero (eee>0); in addition, a greater amplitude was presented in the inverter output voltage signal (168 V) versus the magnitude of the reference signal (155.5 V) when nonlinear load was supplied. With the PI controller implementation, feeding non-linear load, a total harmonic distortion of the voltage signal (THDv) of 10.7 % is presented; value higher than that recommended by regulations, which is 5 %.

On the other hand, with the P+GI controller implementation, it was observed that this presented an setpoint tracking error equal to zero (eee=0), in addition, the amplitude of the inverter output voltage signal and the reference signal presented the same value (155.5 V) when feeding non-linear load. With this controller, the inverter performance was considerably improved, since when supplying non-linear load the THDv was reduced from 10.7% to 5.4 %; and with the design of generalized integrators at the frequencies of the third and fifth load harmonics, the THDv was reduced to 2.2 %.

Finally, when the inverter underwent load changes, it exhibited good performance since it was observed that for a change the load from its nominal value 12.96 A peak to peak at 0 A, the inverter output voltage remained constant. Also, when one inverter phase reduced its load to zero (i=0), the current was conducted by the neutral wire, keeping the voltage signals unchanged in amplitude (155.5 V) and frequency (60 Hz). This behavior with load changes was similar with the implementation of the PI controller.

As future work it is recommended to develop the inverter for its grid-connected operation.

REFERENCES

[1] P.-Y. Kong, "Effects of communication network performance on dynamic pricing in smart power grid," *IEEE Syst. J.*, vol. 8, no. 2, pp. 533–541, Jun. 2014.

[2] S. Parhizi, H. Lotfi, A. Khodaei, and S. Bahramirad, "State of the art in research on microgrids: A review," *IEEE Access*, vol. 3, pp. 890–925, 2015.

[3] T. Kerdphol, F. S. Rahman, Y. Mitani, M. Watanabe, and S. Kufeoglu, "Robust virtual inertia control of an islanded microgrid considering high penetration of renewable energy," *IEEE Access*, vol. 6, pp. 625–636, 2018.

[4] Y. Jin, J. Gu, N. Wang, and Y. Wen, "A systemic scheme for improving microgrids' reliability under distribution network fault condition by adopting microgrids-interconnection," in *Proc. China Int. Electr. Energy Conf. (CIEEC)*, Oct. 2017, pp. 87–91.

[5] E. Heydari, M. P. Moghaddam, and A. Y. Varjani, "Multi-resonant dual loop control of stand-alone four-leg inverter for microgrids applications," in *Proc. 9th Annu. Power Electron., Drives Syst. Technol. Conf. (PEDSTC)*, Feb. 2018, pp. 352–357.

[6] J. Roark, D. Weng, and A. Maitra, "Measuring the value of microgrids: A benefit-cost framework," *CIRED Open Access Proc. J.*, vol. 2017, no. 1, pp. 1892–1894, Oct. 2017.

[7] C. Sun, G. Joos, and F. Bouffard, "Control of microgrids with distributed energy storage operating in islanded mode," in *Proc. IEEE Electr. Power Energy Conf. (EPEC)*, Oct. 2017, pp. 1–7.

[8] T. Tameghe, R. Wamkeue, I. Kamwa, G. Joos, and M. Ouhrouche, "An enhanced current control scheme for microgrids supporting inverters applications," in *Proc. IECON 43rd Annu. Conf. IEEE Ind. Electron. Soc.*, Oct. 2017, pp. 6375–6379.

[9] G. Masson, I. Kaizuka, J. Lindahl, A. Jaeger-Waldau, G. Neubourg, P. Ahm, J. Donoso, and F. Tilli, "A snapshot of global PV markets—The latest survey results on PV markets and policies from the IEA PVPS programme in 2017," in *Proc. IEEE 7th World Conf. Photovoltaic Energy Convers. (WCPEC) (Joint Conf. 45th IEEE PVSC, 28th PVSEC 34th EU PVSEC)*, Jun. 2018, pp. 3825–3828.

[10] M. A. Matin and D. Divsalar, "Digital state feedback control of a three phase sinusoidal PWM inverter," in *Proc. 33rd IEEE Conf. Decis. Control*, Dec. 1994, pp. 615–616.

[11] S. Ei-Barbari and W. Hofmann, "Digital control of a four-leg inverter for standalone photovoltaic systems with unbalanced load," in *Proc. 26th Annu. Conf. IEEE Ind. Electron. Soc. IECON IEEE Int. Conf. Ind. Electron., Control Instrum. 21st Century Technol.*, Nagoya, Japan, Oct. 2000, pp. 729–734.

[12] E. Avci and M. Ucar, "SRF based output voltage control of 3-level 3-phase 4-leg AT-NPC inverter," *J. Polytech.*, vol. 21, pp. 961–966, Jan. 2018.

[13] M. Pichan, H. Rastegar, and M. Monfared, "Deadbeat control of the stand-alone four-leg inverter considering the effect of the neutral line inductor," *IEEE Trans. Ind. Electron.*, vol. 64, no. 4, pp. 2592–2601, Apr. 2017.

[14] L. Hassaine, E. OLias, J. Quintero, and V. Salas, "Overview of power inverter topologies and control structures for grid connected photovoltaic systems," *Renew. Sustain. Energy Rev.*, vol. 30, pp. 796–807, Feb. 2014.

[15] M. R. Miveh, M. F. Rahmat, A. A. Ghadimi, and M. W. Mustafa, "Control techniques for three-phase four-leg voltage source inverters in autonomous microgrids: A review," *Renew. Sustain. Energy Rev.*, vol. 54, pp. 1592–1610, Feb. 2016.

[16] I. Vechiu, H. Camblong, G. Tapia, B. Dakyo, and O. Curea, "Control of four leg inverter for hybrid power system applications with unbalanced load," *Energy Convers. Manage.*, vol. 48, no. 7, pp. 2119–2128, Jul. 2007.

[17] M. Savaghebi, A. Jalilian, J. C. Vasquez, and J. M. Guerrero, "Autonomous voltage unbalance compensation in an islanded droop-controlled microgrid," *IEEE Trans. Ind. Electron.*, vol. 60, no. 4, pp. 1390–1402, Apr. 2013.

[18] D. N. Zmood, D. G. Holmes, and G. H. Bode, "Frequency-domain analysis of three-phase linear current regulators," *IEEE Trans. Ind. Appl.*, vol. 37, no. 2, pp. 601–610, 2001.

[19] A. Timbus, M. Liserre, R. Teodorescu, P. Rodriguez, and F. Blaabjerg, "Evaluation of current controllers for distributed power generation systems," *IEEE Trans. Power Electron.*, vol. 24, no. 3, pp. 654–664, Mar. 2009.

[20] M. S. Munsi, A. B. Siddique, S. K. Das, S. K. Paul, M. R. Islam, and M. A. Moni, "A novel blended state estimated adaptive controller for voltage and current control of microgrid against unknown noise," *IEEE Access*, vol. 7, pp. 161975–161995, 2019.

[21] A. Gastalver-Rubio, E. Romero-Ramos, and J. M. Maza-Ortega, "Improving the performance of low voltage networks by an optimized unbalance operation of three-phase distributed generators," *IEEE Access*, vol. 7, pp. 177504–177516, 2019.

[22] D. N. Zmood and D. G. Holmes, "Stationary frame current regulation of PWM inverters with zero steady-state error," *IEEE Trans. Power Electron.*, vol. 18, no. 3, pp. 814–822, May 2003.

[23] M. Arab, A. Zegaoui, P. Petit, A. Djahbar, and M. Aillerie, "Output-voltage feedback control topology for inverters dedicated to renewable energy systems," *Int. J. Circuit Theory Appl.*, vol. 45, no. 12, pp. 2270–2280, Dec. 2017.

[24] J.-M. Wang, P.-J. Tseng, S.-C. Yen, P.-J. Liu, and H.-J. Chiu, "A new digital control method for a voltage source inverter to compensate for imbalance of output voltage," *Int. J. Circuit Theory Appl.*, vol. 41, no. 8, pp. 879–888, Aug. 2013, doi: 10.1002/cta.1808.

[25] K. Ogata, *Modern Control Engineering*, 5th ed. Upper Saddle River, NJ, USA: Prentice-Hall, Sep. 2009.

[26] G. Tsirimokou, C. Psychalinos, and A. S. Elwakil, "Fractional-order electronically controlled generalized filters," *Int. J. Circuit Theory Appl.*, vol. 45, no. 5, pp. 595–612, May 2017.

[27] I. Serban, "Harmonic compensation with active loads designed for power quality improvement in microgrids," in *Proc. Int. Conf. Develop. Appl. Syst. (DAS)*, May 2018, pp. 120–125.

[28] M. Pichan, G. Arab Markadeh, and F. Blaabjerg, "Continuous finite-time control of four-eg inverter through fast terminal sliding mode control," *Int. Trans. Electr. Energy Syst.*, vol. 30, no. 6, Jun. 2020, Art. no. e12355, doi: 10.1002/2050-7038.12355.

[29] S. Bifaretti, A. Lidozzi, L. Solero, and F. Crescimbini, "Comparison of modulation techniques for active split DC-bus three-phase four-leg inverters," in *Proc. IEEE Energy Convers. Congr. Expo. (ECCE)*, Sep. 2014, pp. 5631–5638.

[30] E. Ebrahimzadeh, S. Farhangi, H. I. Eini, and F. Blaabjerg, "Modulation technique for four-leg voltage source inverter without a look-up table," *IET Power Electron.*, vol. 9, no. 4, pp. 648–659, Mar. 2016.

[31] A. Lidozzi, C. Ji, L. Solero, P. Zanchetta, and F. Crescimbini, "Resonant-repetitive combined control for stand-alone power supply units," *IEEE Trans. Ind. Appl.*, vol. 51, no. 6, pp. 4653–4663, Nov.-Dec. 2015.

[32] V. Yaramasu, B. Wu, M. Rivera, and J. Rodriguez, "Enhanced model predictive voltage control of four-leg inverters with switching frequency reduction for standalone power systems," in *Proc. 15th Int. Power Electron. Motion Control Conf. (EPE/PEMC)*, Sep. 2012, Art. no. 6397290.

[33] V. Yaramasu, M. Rivera, M. Narimani, B. Wu, and J. Rodriguez, "Model predictive approach for a simple and effective load voltage control of four-leg inverter with an output *LC* filter," *IEEE Trans. Ind. Electron.*, vol. 61, no. 10, pp. 5259–5270, Oct. 2014.

[34] E. Demirkutlu and A. M. Hava, "A scalar resonant-filter-bank-based output-voltage control method and a scalar minimum-switching-loss discontinuous PWM method for the four-leg-inverter-based three-phase four-wire power supply," *IEEE Trans. Ind. Appl.*, vol. 45, no. 3, pp. 982–991, May./Jun. 2009.

[35] X. Zhang, J. Wang, and C. Li, "Three-phase four-leg inverter based on voltage hysteresis control," in *Proc. Int. Conf. Electr. Control Eng.*, Jun. 2010, pp. 4482–4485.

[36] K. M. Santosh, V. B. Borghate, R. R. Karasani, S. Sabyasachi, and H. M. Suryawanshi, "A fault-tolerant modular multilevel inverter topology," *Int. J. Circuit Theory Appl.*, vol. 46, no. 5, pp. 1028–1043, 2018.

VIRGILIO VÁSQUEZ received the B.Sc. and Ph.D. degrees in electrical engineering from the Centro de Investigación y de Estudios Avanzados del Instituto Politécnico Nacional (Cinvestav), Mexico City, Mexico, 1997 and 2005, respectively. He has been a Professor with Tecnológico de Monterrey, since 1997. His main research fields are in modeling and control of electric machines applied to the distributed generation and distributed control systems.

RUBÉN ORTEGA received the B.Sc. degree in electrical engineering, in 1999, and the M.Sc. degree in systems engineering from the Instituto Politécnico Nacional, Ciudad de Mexico, Mexico, and the D.E.A. degree in electrical engineering, computer, and electronic system from the Universidad de Oviedo, Oviedo, Spain, in 2009. He is currently pursuing the Ph.D. degree with the Universidad Politécnica de Valencia, Valencia, Spain. He has been a Professor with the Department of Computer Science and Engineering, Escuela Superior de Cómputo, Instituto Politécnico Nacional, since 1995. His main research fields are in modeling and control of power converters applied to the distributed generation in microgrids and digital signal processing.

LUIS MAURO ORTEGA received the B.Sc. degree in electrical engineering from the Centro de Investigación y Estudios Avanzados (CINVESTAV) del Instituto Politécnico Nacional, Mexico City, Mexico, 1996, and the Ph.D. degree in electric engineering from the Instituto Politécnico Nacional. He has been a Professor with Tecnológico de Monterrey, since 1998. His main research field are in modeling and control of power electric systems applied to the control and generation of electric energy.

VÍCTOR HUGO GARCÍA received the Engineering degree in computation systems and the M.Sc. degree from the Instituto Politecnico Nacional, Mexico City, Mexico, in 1999 and 2006, respectively. He is currently a Professor of computer architecture with the Escuela Superior de Computo, Instituto Politecnico Nacional, Mexico City, since 2004. His current research interests are computer architecture, signal and image processing, and embedded systems.

OSCAR CARRANZA (Member, IEEE) received the B.S. degree in communication and electronics engineering and the M.Sc. degree in electronics engineering from the Instituto Politécnico Nacional, Mexico City, Mexico, in 1996 and 1999, respectively, and the Ph.D. degree in electronics engineering from the Universidad Politécnica de Valencia, Valencia, Spain, in 2012. He has been a Professor with the Escuela Superior de Computo, Instituto Politecnico Nacional, since 1999. His main research fields are in modeling and control of power converters, power processing of renewable energy sources, and grid-connected converters for distributed power.